Superconductivity

Y. Xiao, Y. Su

This document has been published in

Manuel Angst, Thomas Brückel, Dieter Richter, Reiner Zorn (Eds.):
Scattering Methods for Condensed Matter Research: Towards Novel Applications at Future Sources
Lecture Notes of the 43rd IFF Spring School 2012
Schriften des Forschungszentrums Jülich / Reihe Schlüsseltechnologien / Key Technologies, Vol. 33
JCNS, PGI, ICS, IAS
Forschungszentrum Jülich GmbH, JCNS, PGI, ICS, IAS, 2012
ISBN: 978-3-89336-759-7

E 1 Superconductivity [1]

Y. Xiao and Y. Su
Jülich Centre for Neutron Science
Forschungszentrum Jülich GmbH

Contents

---

[1] Lecture Notes of the 43rd IFF Spring School "Scattering Methods for Condensed Matter Research: Towards Novel Applications at Future Sources" (Forschungszentrum Jülich, 2012). All rights reserved.

1 Introduction

Superconductivity is an exotic state of matter that has fascinated generations of scientists ever since its discovery in mercury in 1911 [1]. After more than 100 years, there are whole classes of superconducting materials that we still do not fully understand. In particular, understanding the mechanism of high temperature superconductivity in cuprates, discovered in 1986 by Bednorz and Müller [2], and in recently discovered iron-based superconductors [3] has remained as one of the hardest tasks in condensed matter physics.

In this lecture note, the fundamentals of superconductivity, as commonly covered in most textbooks on solid state physics, will be given first. Detailed descriptions on the phenomenon of superconductivity, phenomenological theories i.e. the London theory and Ginzburg-Landau theory and the landmark microscopic BCS theory can be found in this section. A brief overview of large classes of the known superconducting materials, including both conventional and unconventional superconductors will be given as well. The high temperature superconductivity is a vast and always rapidly moving field, it is neither in our intention nor possible to present a comprehensive review on the current status as well as a thorough description of the underlying physics. Therefore, only some important aspects and basic understanding of the recently discovered iron-based superconductors will be discussed here. The choice of the covered topic is more or less based on our own research activities in this field with the main focus on the neutron scattering studies.

2 Fundamentals of Superconductivity

2.1 Zero resistivity

In order to explain the electronic property of metals, the Drude theory was developed by Drude in 1900. In the framework of the Drude theory, electrons are treated as classical particles. When electrons are moving through the solid, they will collide with scattering center and change their direction and velocity. In a metal, the conductivity can be defined by the constitutive equation as the proportionality between electrical current density **J** and electric field **E**: $\mathbf{J}=\sigma\mathbf{E}$. The electrical conductivity σ is given by Drude theory as:

$$\sigma = \frac{ne^2\tau}{m} \tag{1}$$

where τ is the mean life time and *m* is the effective mass of the conduction electrons. The resistivity ρ is the reciprocal of the conductivity. *i.e.* $\rho = 1/\sigma$ and $\rho \propto \tau^{-1}$. The resistivity is the sum of the contributions from different scattering processes. The scattering mechanisms can be impurity scattering, electron-electron scattering and electron-phonon scattering. Furthermore, these scattering processes act independently and they have different mean life times. The total resistivity reads:

$$\rho = \frac{m}{ne^2}(\tau_i^{-1} + \tau_{e-e}^{-1} + \tau_{e-p}^{-1}) \tag{2}$$

The temperature dependencies of these mean life times are also different. The impurity scattering life time is independent of temperature, while the lifetimes of electron-electron and electron-phonon scattering will exhibit temperature variation. At low temperatures, electron-electron scattering and electron-phonon scattering are negligible. Therefore, one expects a constant value for resistivity at zero temperature as the residual resistivity.

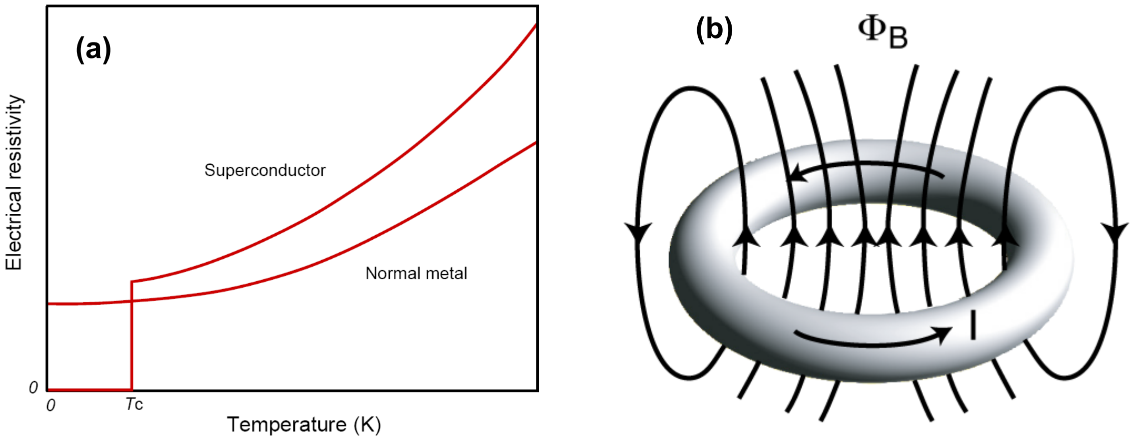

Fig. 1: *(a): Temperature dependence of the electrical resistivity for superconductors and normal metals. (b): The superconducting current maintains through the superconducting ring [4, 5].*

In 1911, Heike Kamerlingh Onnes performed an experiment to test the validity of the Drude theory by measuring the resistivity of mercury at low temperature. Surprisingly, he found the electrical resistance dropped sharply to zero below 4.2 K [1]. Thus the superconductivity was discovered and it represents a new state of matter [4, 5].

As shown in Fig. 1(a), the resistivity of superconductor drops to zero when temperature is below the critical temperature T_c. However, due to the experimental difficulty, we are not be able to measure the zero resistivity. The existence of persistent current in a closed loop of superconducting wire can be considered as the strong evidence of superconductivity. As shown in Fig. 1(b), a circulating current I can be introduced in the superconducting ring. If the superconductor has the zero resistivity, the energy stored in the ring will keep constant and the current will continue flowing in the ring. Experimentally, it was found that almost no detectable decay of the current in superconducting ring for years.

2.2 Meissner effect

Suppose we take a superconductor and place it under magnetic field, the external magnetic field will penetrate into the superconductor if the superconductor is in its normal state, *i.e.* $T > T_c$. Then we will get almost same value of magnetic field inside and outside of superconductor as indicated in Fig. 2(a). When we cool the superconducting sample below T_c in the presence of the same field, the magnetic field will be expelled from the sample. This phenomenon was discovered by Meissner in 1933 and named as Meissner effect [6].

As we known, the superconductor exhibits zero resistivity. By $\mathbf{E} = \rho\mathbf{J}$, we will have $\mathbf{E} = 0$ inside of superconductor. By using the Maxwell equation $\nabla\times\mathbf{E} = -\partial\mathbf{B}/\partial t$, we got $\partial\mathbf{B}/\partial t = 0$. It is also known that magnetic flux density $\mathbf{B}$ is related with magnetic field $\mathbf{H}$ and magnetization of sample $\mathbf{M}$ by $\mathbf{B} = \mu_0(\mathbf{H}+\mathbf{M})$. Eventually, we find that $\partial\mathbf{M}/\partial\mathbf{H} = \chi = -1$ for superconductor. Susceptibility $\chi = -1$ indicated that the superconductors possess perfect diamagnetism. To study the magnetic susceptibility as a function of temperature, we will be able to characterize the

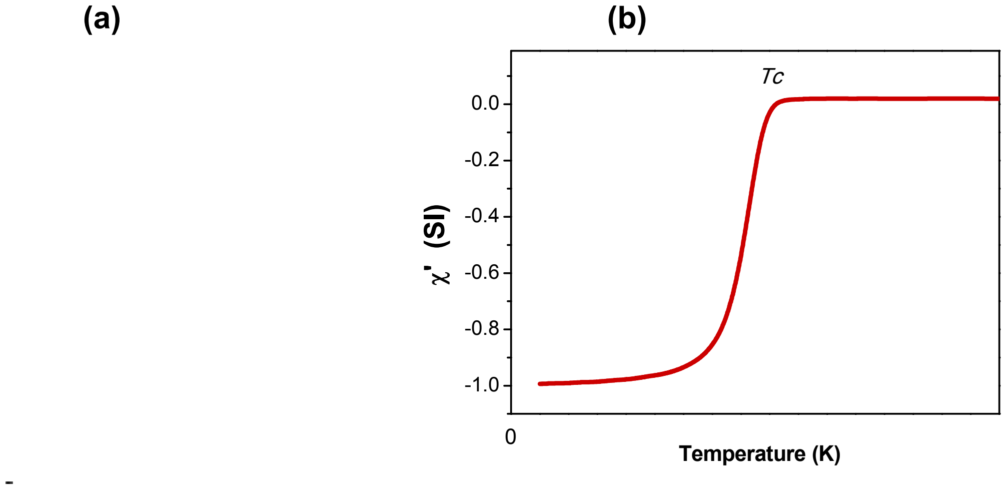

Fig. 2: *(a): The Meissner effect in superconductors. (b): Temperature dependence of susceptibility (χ) of bulk superconductor [4, 5].*

superconducting sample. As shown in Fig. 2(b), we will obtain χ = -1 for bulk superconductor below T_c, which is the solid evidence for Meissner effect.

2.3 London theory

In 1935, London brothers developed the first theory to explain the magnetic properties of superconductors [7]. By applying the two-fluid model, the 1^{st} London equation can be obtained, which relate the superconducting current density **J** with the electric field **E**:

$$\mathbf{E} = \mu_0 \lambda_L^2 \frac{\partial \mathbf{J}}{\partial t} \tag{3}$$

Combination of Eq. (3) with Maxwell equation $\nabla \times \mathbf{E}$ = -$\partial \mathbf{B}/\partial t$, London equation can also be rewritten in terms of magnetic field **B** and superconducting current density **J**, which is called 2^{nd} London equation:

$$\mathbf{B} = -\mu_0 \lambda_L^2 \nabla \times \mathbf{J} \tag{4}$$

In both Eq. (3) and Eq. (4), λ_L is the London penetration depth with the dimension of length,

$$\lambda_L = (\frac{m_e}{\mu_0 n_s e^2})^{1/2} \tag{5}$$

The London equations provide a simple phenomenological model to explain the Meissner effect. It also implies that the magnetic field will only penetrate the surface layer of depth λ_L and the field equals to zero inside the bulk superconductor.

2.4 Ginzburg-Landau theory

In 1930, Landau had developed a theory for second-order phase transition. Many second-order phase transitions can be characterized by an appropriate order parameter, the order parameter shows different value at high temperature disordered state and low temperature order state. For example, the magnetic order parameter is always used to describe the magnetic phase transition from ferromagnetism to paramagnetism. In 1950, Ginzburg and Landau proposed to describe the superconducting state with a more complex order parameter Ψ, here Ψ is spatially varied, and $|\Psi|^2$ is proportional to the density of super electrons, *i.e.* $|\Psi|^2 = n_s(r)$. Ψ is nonzero in the superconducting state, while it equals zero in normal state above critical temperature T_c [8]. Since superconducting state is a thermal equilibrium state, its thermal dynamic property can be described with free energy density f_s. For temperature close to critical temperature, free energy can be expanded as a function of order parameter $|\Psi|$,

$$f_s(T) = f_n(T) + a(T)|\Psi|^2 + \frac{b(T)}{2}|\Psi|^4 + \cdots \tag{6}$$

where $f_s(T)$ is the free energy density of the normal state, a and b are the temperature dependent parameters, In order to get minimum for f_s, *b(T)* has to be positive, while *a(T)* can be either positive or negative, corresponding to $T > T_c$ or $T < T_c$, respectively. If we plot the difference of free energy density as a function of Ψ, we will get two different curves for $a(T) > 0$ and $a(T) < 0$. These two curves have different minimum: at $\Psi = 0$ for $T > T_c$ and at $|\Psi|^2 = -a(T)/b(T)$ for $T < T_c$.

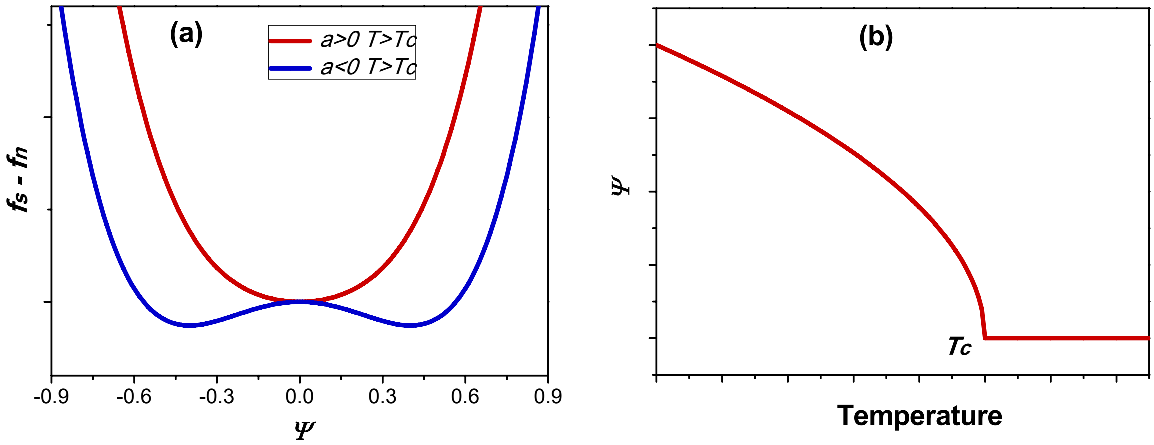

Fig. 3: *(a): Difference between the free energy in the normal and superconducting state as a function of order parameter Ψ. (b): Temperature dependence of order parameter Ψ in superconductor.*

In a spatially inhomogeneous superconductor, the order parameter depends on position. A new term depending on the gradient of $\Psi(r)$ should be included in the free energy. If we also consider the effect of magnetic field $\mathbf{B} = \mu_0\mathbf{H}$, another additional term should also be included. Therefore the free energy of superconductor in the magnetic field is:

$$f_s(T) = f_n(T) + a|\Psi|^2 + \frac{b}{2}|\Psi|^4 + \frac{1}{2m_s}|(-i\hbar\nabla - 2eA)\Psi|^2 + \mu_0\frac{|H|^2}{2} \tag{7}$$

By minimizing the free energy of the system, we can get two Ginzburg-Landau equations:

$$a\Psi + b|\Psi|^2\Psi + \frac{1}{2m_s}(-i\hbar\nabla - 2eA)^2\Psi = 0 \tag{8}$$

$$\mathbf{J}_s = -\frac{2e\hbar i}{i2m_s}(\Psi^*\nabla\Psi - \Psi\nabla\Psi^*) - \frac{(2e)^2}{m_s}|\Psi|^2 A \tag{9}$$

Suppose there exists an interface between normal state and superconducting state. By assuming that $\Psi(r)$ is continuous and the boundary condition at $\Psi(0) = 0$, we can solve the first Ginzburg-Landau equation and get $\Psi(r)$:

$$\Psi(r) = \Psi(0)tanh(\frac{r}{\sqrt{2}\xi(T)}) \tag{10}$$

where $\Psi(0)$ is the order parameter far from the interface in the superconducting and $\xi(T)$ is called Ginzburg-Landau coherence length:

$$\xi(T) = \sqrt{\frac{\hbar^2}{2m_s|a(T)|}} \tag{11}$$

Beside of the London penetration depth λ_L, Ginzburg-Landau coherence length $\xi(T)$ is another fundamental length scale associated with superconductivity. The ratio between these two length scales is denoted as Ginzburg-Landau parameter, which is independent of temperature,

$$\kappa = \frac{\lambda(T)}{\xi(T)} \tag{12}$$

Usually, the ratio $\kappa = 1/\sqrt{2}$ is adopted as the criterion to define the type-I and type-II superconductors:

$$\kappa \leq 1/\sqrt{2} \qquad (Type - I) \tag{13}$$

$$\kappa \geq 1/\sqrt{2} \qquad (Type - II) \tag{14}$$

For type-I superconductor, the field inside is zero due to the Meissner effect, when external field is larger than critical field H_c, the superconductivity is destroyed suddenly. While, there are two different critical fields in type-II superconductor: the lower critical field H_{C1} and upper critical field H_{C2}. If external field is smaller than H_{C1}, the sample is perfect diamagnet. If external field exceeds H_{C1} but below H_{C2}, the superconductor enters the so called Shubnikov phase, in which the magnetic flux penetrates the superconductor in the form of vortices [9]. If external field increases further, the vortex cores are getting closer and almost overlap when external field reached upper critical field H_{C2}. The superconductivity will be totally destroyed once the field exceeds H_{C2}.

2.5 Electron-pairing and the BCS theory

As a phenomenological theory, the Ginzburg-Landau theory was quite successful in explaining many physical properties of superconductor. However, it can not explain the microscopic origins of superconductivity. For instance, the physical meaning of the Ginzburg-Landau order parameter was still no clear. In 1957, Bardeen, Cooper, and Schrieffer (BCS) proposed a microscopic theory which can provide the physical interpretation of the nature of order parameter and describe the macroscopic wavefunction of conduction electrons [10]. The key idea of BCS theory is that the crystal lattice phonons can act as the exchange bosons and give an attractive interaction between the conduction electrons near the Fermi surface. Thus, the pair bound state of electrons is formed and the paired conduction electrons are called "Cooper pair".

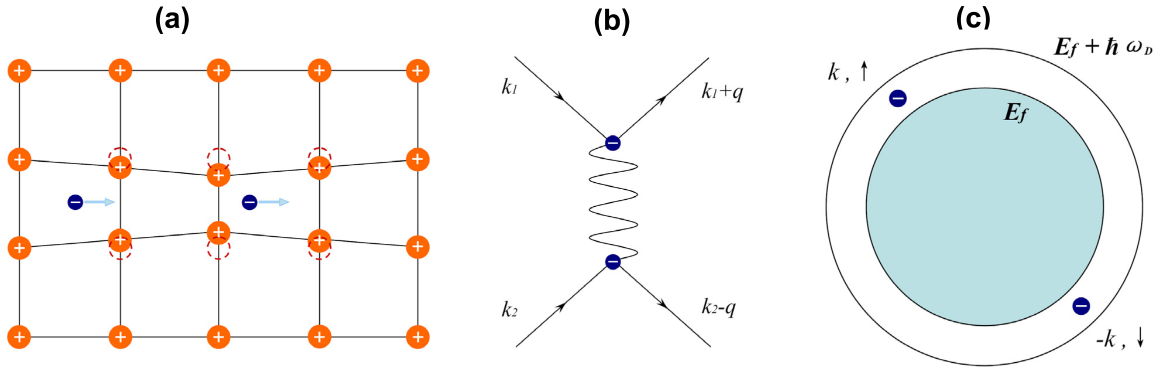

Fig. 4: *(a) Two electrons paired when moving through crystal lattice due to the electron phonon coupling. (b) Interaction of electrons via exchange of boson (crystal lattice phonon). (c) Attractive interaction between two electrons close to the Fermi surface.*

It is well known that bare electrons will repel each other due to the strong electrostatic Coulomb repulsion. However, if we consider the electrons in a medium, say, surrounded by charged ions in a crystal lattice [Fig. 4(a)], the Coulomb interaction will be largely reduced by the screening. Furthermore, the attractive electron-electron interaction is generated via the exchange of virtual exchange bosons such as phonons. As presented in Fig. 4(b), the Feynman diagram illustrated the interaction of electrons via exchange phonons. Because the total wave vector is conserved, we have k_1+k_2 = k_1+q+k_2-q = k'_1+k'_2. Considering a situation that only two additional electrons located outside of the spherical Fermi surface at T = 0. The interaction between two additional electrons will take place within the range $\hbar\omega_D$ of Fermi surface, *i.e.* $E_f < E_k < E_f$+$\hbar\omega_D$. To ensure the momentum conservation and to minimize the energy, two additional electrons will pair up as Cooper pair with no center of mass motion, as demonstrated in Fig. 4(c).

The coupling of the electron spins of the Cooper pairs will result in two different total spin, S = 0 or S = 1. Thus the spin wave function can be:

$$\phi = \frac{1}{\sqrt{2}}(|\uparrow\downarrow\rangle - |\downarrow\uparrow\rangle) \qquad (S = 0, singlet) \tag{15}$$

$$or \quad \phi = \begin{cases} |\uparrow\uparrow\rangle \\ \frac{1}{\sqrt{2}}(|\uparrow\downarrow\rangle + |\downarrow\uparrow\rangle) \\ |\downarrow\downarrow\rangle \end{cases} \qquad (S = 1, triplet) \tag{16}$$

Furthermore, based on the distribution of pairing amplitude in k space, the pairing symmetry can be classified as *s, p, d, f*...waves.

By using the language of second quantization, the pairing hamiltonian of singlet superconductor can be given as:

$$\mathcal{H} = \sum_{k,\sigma} \epsilon(k) n_{k\sigma} + \sum_{k,k'} V_{k,k'} c^\dagger_{k\uparrow} c^\dagger_{-k\downarrow} c_{-k'\downarrow} c_{k'\uparrow} \tag{17}$$

By defining $b_k = \langle c_{-k\downarrow} c_{k\uparrow} \rangle$ and $\triangle_k = -\sum\limits_{k'} V_{k,k'} \langle c_{-k\downarrow} c_{k\uparrow} \rangle$, the model Hamiltonian is expressed as:

$$\mathcal{H} = \mu N + \sum_{k,\sigma} \xi_k c^\dagger_{k\sigma} c_{k\sigma} - \sum_k (\triangle_k c^\dagger_{k\uparrow} c^\dagger_{-k\downarrow} + \triangle^*_k c^\dagger_{-k\downarrow} c^\dagger_{k\uparrow}) \tag{18}$$

The above Hamiltonian can be diagonalized by Bogoliubov-Valatin transformation:

$$c_{k\uparrow} = u^*_k \gamma_{k\uparrow} + v_k \gamma^\dagger_{-k\downarrow} \tag{19}$$

$$c^\dagger_{k\uparrow} = -v^*_k \gamma_{k\uparrow} + u_k \gamma^\dagger_{-k\downarrow} \tag{20}$$

with $|u_k|^2 + |v_k|^2 = 1$.

If we insert these operators into the model Hamiltonian, use the relation between u_k and v_k, then properly choose u_k and v_k, the following relations will be obtained:

$$2\xi_k u_k v_k + \triangle^*_k v^2_k - \triangle_k u^2_k = 0 \tag{21}$$

Simplify above equation by multiple $\triangle^*_k / u^2_k$ to both two sides gives:

$$\frac{\triangle^*_k v_k}{u_k} = \sqrt{\xi^2_k + |\triangle_k|^2} - \xi_k \tag{22}$$

Excitation energy E_k is defined as $E_k = \sqrt{\xi^2_k + |\triangle_k|^2}$ [Fig. 5(a)], thus, v_k and u_k can be expressed in term of E_k as:

$$|v_k|^2 = 1 - |u_k|^2 = \frac{1}{2}(1 - \frac{\xi}{E_k}) \tag{23}$$

In BCS theory, Bardeen, Cooper and Schrieffer proposed the ground state as:

$$|\Psi_G\rangle = \prod_k (u_k + v_k c^\dagger_{k\uparrow} c^\dagger_{-k\downarrow})|0\rangle \tag{24}$$

Noted that $|u_k|^2 + |v_k|^2 = 1$. This implies that the parameter u_k and v_k are the probability amplitudes. The probability of the pair ($k\uparrow$,$-k\downarrow$) being occupied is $|v_k|^2$, while the probability of the pair being unoccupied is $|u_k|^2$. The relations between occupation probability $|v_k|^2$ and $|u_k|^2$ is shown in Fig. 5(b).

The ground state energy can be expressed as:

$$\langle E_G \rangle = \sum_k \left(\xi_k - \frac{\xi^2_k}{E_k} \right) - \frac{\Delta^2}{V_0} \tag{25}$$

Because the occupation probability is given by the Fermi-Dirac distribution, the definition of $\triangle_k$ can be rewritten as:

$$\begin{aligned} \triangle_k &= -\sum_{k'} V_{k,k'} \langle c_{-k\downarrow} c_{k\uparrow} \rangle \\ &= -\sum_{k'} V_{k,k'} u_{k'} v_{k'} (1 - 2f(E_{k'})) \\ &= -\sum_{k'} V_{k,k'} \frac{\triangle_{k'}}{2E_{k'}} tanh \left(\frac{E_{k'}}{2k_B T} \right) \end{aligned} \tag{26}$$

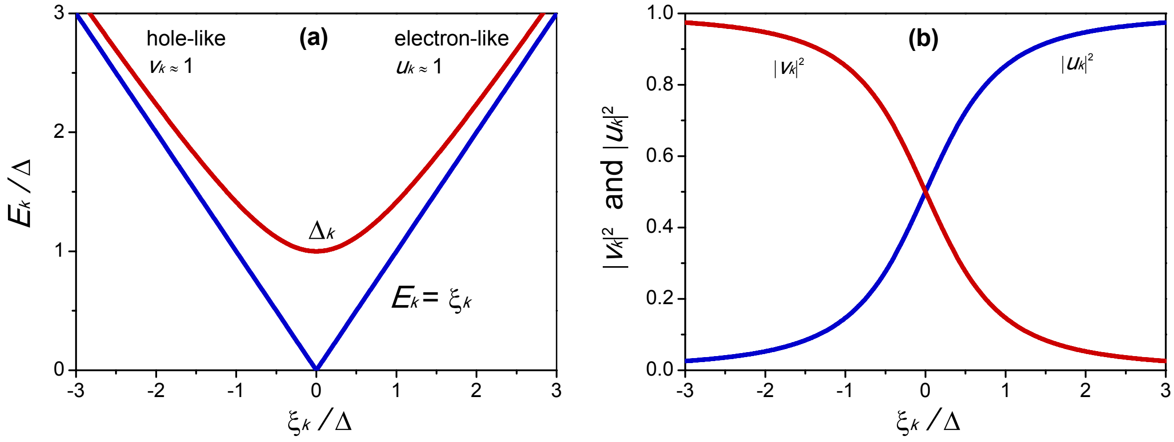

Fig. 5: *(a) Excitation energy E_k as a function of ξ_k in the normal and superconducting state. (b) Occupation probability $|v_k|^2$ and $|u_k|^2$ as a function of ξ_k at T = 0 near the Fermi level.*

Based on the assumption of week coupling in BCS theory, *i.e.* $V_{k,k'} = -V_0$, $\triangle_{k'} = \triangle$, the summation of above equation can be converted into an integration over energy, then we arrive at the BCS gap equation:

$$1 = \lambda \int_0^{\hbar\omega_D} \frac{1}{E_k} tanh \left(\frac{E_k}{2k_BT} \right) d\xi_k \tag{27}$$

where $\lambda = V_0 D(\mu)$ is the dimensionless electro-phonon coupling constant, $D(\mu)$ is the density of states. The BCS gap equation gives the temperature dependence of gap energy, in particular, it gives not only the energy gap at zero temperature but also the ordering temperature T_c.
For temperature approaching to T_c, we have $\triangle \to 0$. Then we can get the equation for the critical temperature:

$$k_BT_c = 1.13\hbar\omega_D e^{-1/\lambda} \tag{28}$$

Also at low temperature the ratio between $\triangle$ and T_c can be determined as

$$\frac{\triangle(0)}{k_BT_c} = 1.764 \tag{29}$$

Above relation is one of the most important result deduced from the BCS theory, indeed, it was obeyed by all classical metallic superconductors as an universal amplitude ratio.

3 A survey of the superconducting materials

After superconductivity was found in Hg with T_c = 4.2 K, great efforts are made to search for new superconductors. Till now, thousands of superconducting materials have been found [11]. However, superconductivity is still a low temperature phenomenon. To find a room-temperature superconductor seems still a long way to go. In the following parts, the main superconducting materials are classified.

- **Superconducting element**

After Hg, Superconductivity is also found in some other elements, such as Sn, Pb and La. Among all elements, Pb possesses the highest T_c of 9.2 K in the ambient pressure. Although some elements are non-superconductor at very low temperature, the superconductivity can emerge when they are subjected to high pressure or fabricated as thin films.

- **Superconducting alloys and compounds**

As a solid solution of different kinds of atoms, some alloys also exhibit superconductivity, such as NbTi (T_c = 9.5 K) and NbTa (T_c = 6.0 K). Higher T_c are also found in other Nb-content A_3B compounds, e.g. T_c = 18 K for Nb_3Sn and T_c = 23.2 K for Nb_3Ge. Besides, the superconductivity with T_c up to 40 K was discover in MgB_2 [12].

- **Organic superconductors**

Usually, the Organic compounds are insulators, but it was found that some organic compounds are superconductors. The Critical temperatures of organic superconductors are still in the range of classical superconductors [13].

- **Heavy-fermion superconductors**

In Heavy-fermion system, the electrons have large effective mass of about 200 times the free electron mass. Superconductivity was found in some heavy-fermion system such as $CeCu_2Si_2$. It was believed that heavy Fermion superconductors belong to the unconventional superconductor, however, the mechanism of this kind of superconductor is still not clear [14].

- **Superconducting fullerene compounds**

Fullerene, with the formula C_{60} was discovered as the third form of carbon in 1980s. After intercalating with exotic atoms, the doped C_{60} molecular crystals will exhibit the superconductivity with T_c up to 40 K [15, 16].

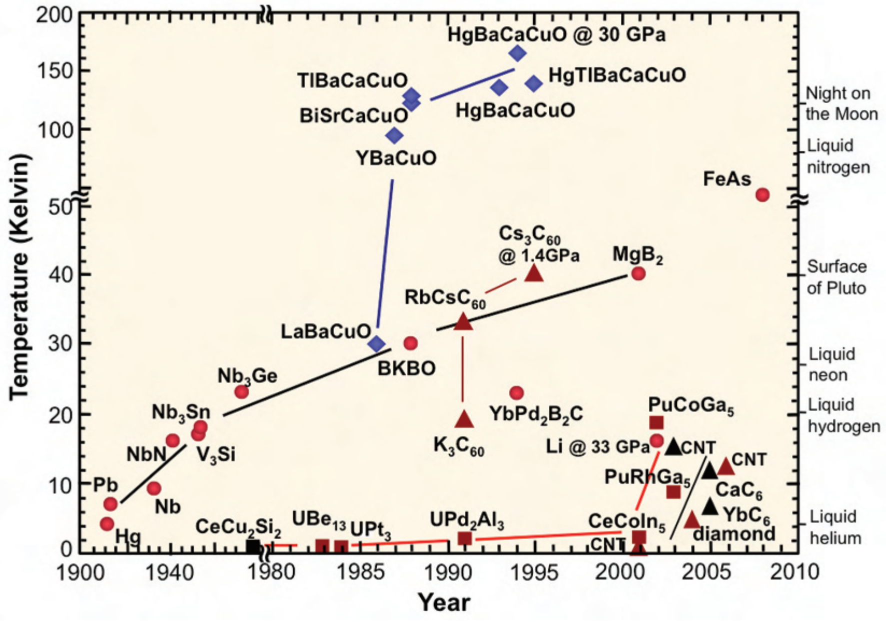

Fig. 6: *Timeline of the discovery of superconductors [17].*

- **High-T_c cuprate superconductors**

In 1986, the first cuprate superconductor $La_{2-x}Ba_xCuO_4$ with $T_c \approx 30$ K was discovered by Bednorz and Müller [2]. It was quite surprising that high T_c is shown in cuprate since the oxidize compounds are always insulators or poor conductors. The researchers are immediately motivated by this breakthrough and start searching for new cuprate compounds with higher T_c. Soon after, the superconductivity is observed in $YBa_2Cu_3O_{6+x}$ with $T_c \approx 90$ K, which is well above the temperature of liquid nitrogen [18]. So far the highest T_c of 133 K at ambient pressure was found in Hg-based cuprate $HgBa_2Ca_2Cu_3O_8$ [19]. Obviously, the Cuprate with high T_c are unconventional superconductors and it can not be explained in the framework of BCS theory. Therefore, new theory is required to explain the physics of the cuprate superconductors. However, the fundamental mechanism of high-temperature superconductivity is still unclear and it was still considered as the topic of the frontier of condensed matter physics.

From the point of view of crystal structure it was found that all high T_c cuprate have a layered structure. All Cuprate have one or more layers of copper oxide (CuO_2) and the CuO_2 layer are spaced by layers containing elements such as lanthanum, barium or yttrium. The schematic view of crystal structure of $YBa_2Cu_3O_7$ is shown in Fig. 7(a). Based on the large number of experimental results the universal phase diagram relating the critical temperature to doping level can be draw Fig. 7(b).

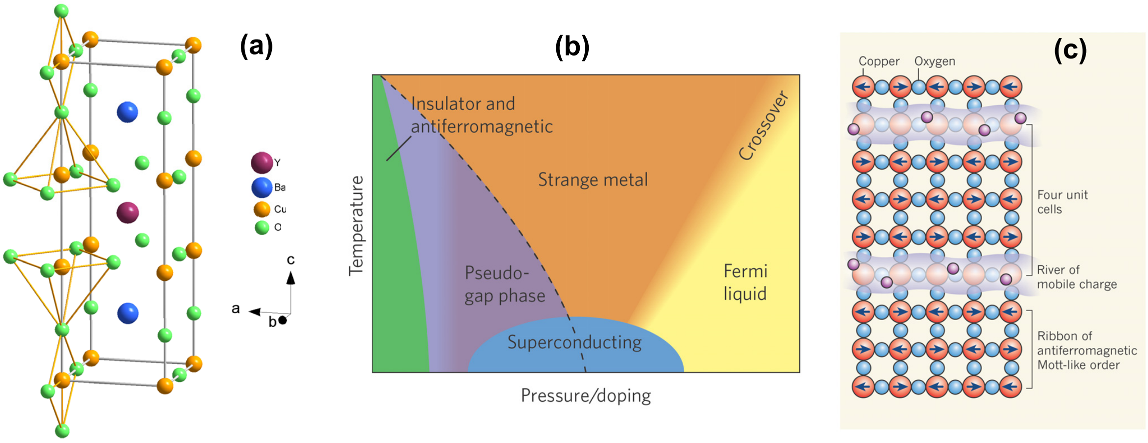

Fig. 7: *(a) Crystal structure of $YBa_2Cu_3O_7$. (b) Schematic phase diagram of hole doped cuprate high T_c cuprate superconductor [20]. (c) Stripe-like electronic order in the cuprates [21].*

Considering the phase diagram with increasing doping, the material is still an antiferromagnetic insulator at the lowest doping level. With increasing doping, the material enters the superconducting phase and the critical temperature T_c exhibits a dome-like dependence on doping with further increases in the doping level. At the over doped level, the material again become non-superconducting. Between the antiferromagnetic and superconducting phase zone, there is phase named pseudogap phase, in which physical properties show behavior of the existence of an energy gap. It is still controversial whether the pseudogap arisen from competing orders or it is the precursor of superconductivity.

As shown in Fig. 7(b), the undoped Cuprate compounds are Mott insulator with long-range antiferromagnetic order of Cu. Upon doping with holes, the stripes of spin and charge order formed. Both charge and spins are periodically modulated in the stripe phase [22]. As illustrated in Fig. 7(c), inhomogeneity arises due to the hole doping process. The antiferromagnetic spin order in the spin-part of stripe is similar as in the undoped antiferromagnetic Mott insulator, whereas the charge can conduct between the spin-part of stripe. Experimentally, the strip phase is directly detected by neutron scattering study. Information on the period of both charge and spin density modulations can be obtained. It was also observed that the period of the charge order is temperature dependent, which indicates the variation of charge concentration as a function of temperature. Theoretically, it was thought that the formation of stripe phase was attributed to the competition between the kinetic energy of the electrons, the antiferromagnetic interaction among spins, and the Coulomb interaction between charges. It was believed that the existence of the strip phase might give rise to superconductivity.

- **Iron-based high-T_c superconductors**

The iron-based superconductors, discovered in 2008 [3], is the latest family of high-T_c superconductors. Extensive attention are drawn afterwards since it provides a new opportunity to investigate the mechanism of unconventional superconductivity. More detailed introductions on iron-based superconductors can be found in the next section.

4 Iron-based high-T_c superconductors

4.1 Materials series and phase diagrams

In 2008, a new family of high-T_c superconductors, iron-based superconductors were discovered [3]. This discovery has provided a new playground to investigate the mechanism of unconventional superconductivity [23]. There are a number of homologous families of iron-based superconductors discovered so far, which are short-named after the stoichiometries of their parent compounds (as shown in Fig. 8(a)). While most of the iron-based superconductors contain arsenic, some contain phosphorus, which come from the same pnictogen group of the periodic table. Therefore, they are usually termed as iron pnictides. In the so-called "11" and "245" families, the pnictogen is replaced by selenium or tellurium from the chalcogen group. These families are thus termed as iron chalcogenides. All iron-based superconductors have a common layer of iron atoms which are tetrahedrally coordinated by pnictogen or chalcogen atoms (as shown in Fig. 8(c)). They differ only in the details of the buffer layers. Experiments and theory now agree that the superconducting electrons in all the iron-based superconductors flow in the planes that contain Fe. Despite of the compositional variety, the Fe-containing planes have the same structure from material to material (as shown in Fig. 8(b)). Note that the iron-containing plane is not flat: pnictogen or chalcogen atoms reside above and below the plane. Because the pnictogen and chalcogen atoms are much larger than the iron atoms, they pack themselves in edge-sharing tetrahedral. By contrast, the smaller size difference between the copper and oxygen atoms in a cuprate superconductor leads to corner-sharing octahedral packing. Such a structural difference has an important consequence on the respective crystal-field splitting and electronic structure.

Most of the research on iron-based superconductors has focused on RFeAs($O_{1-x}F_x$)(with R = La, Nd, Sm, or Pr etc.) and AFe$_2$As$_2$ (with A = Ba, Ca, or Sr etc.), the so-called "1111" and "112" families. Starting from the parent compounds, superconductivity can be achieved either by doping, or by the application of pressure in some materials. Since the parent compounds are already metallic, the effect of the doping can not be solely related to the introduction of free charge carriers. It has been suggested that the modifications of the Fermi surface, which are similar under pressure and chemical doping, are important for inducing superconductivity

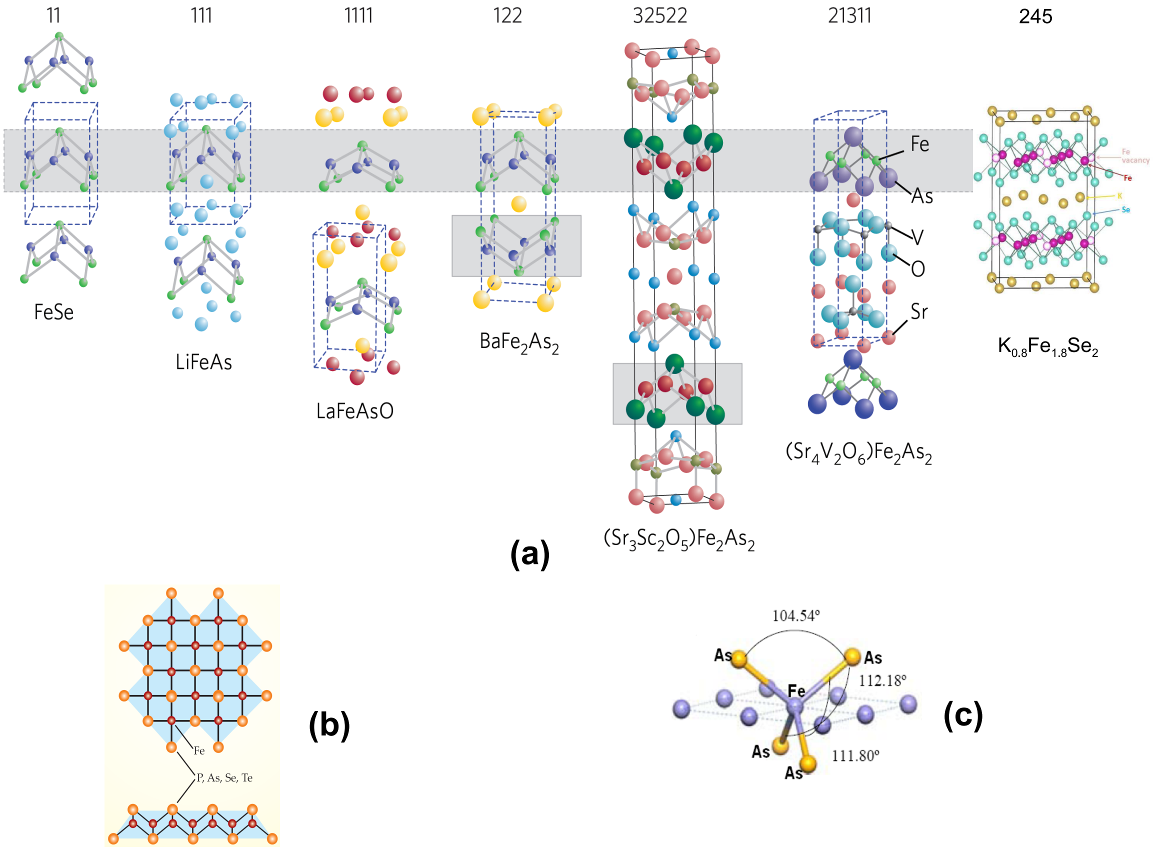

Fig. 8: *(a) Several homologous families of iron-based superconductors [23]; (b) the crystalline plane containing of iron pnictides or iron chalcogenides; (c) the iron atom is tetrahedrally coordinated by pnictogen or chalcogen atoms.*

in the iron-based compounds. Up to now, the highest T_c attained is 57.4 K in the electron-doped '1111' compound $Ca_{0.4}Nd_{0.6}FeAsF$, while for the '122' compound the highest T_c of 39 K is reached in the hole-doped $Ba_{0.6}K_{0.4}Fe_2As_2$. A typical behaviour of the resistivity and magnetization as a function of temperature of the electron-doped $Ba(Fe_{1-x}Co_x))_2As_2$ single crystals is shown in Fig. 9(a)-(b) [24]. The resistivity anomaly at 137 K in the undoped parent 122 compound is due to concurrent phase transitions from tetragonal to orthorhombic and from Pauli paramagnet to low-temperature spin-density wave (SDW) phase. With the increasing of the Co doping level, both orthorhombic structural and SDW phases are suppressed, while superconductivity emerges eventually at higher dpoing levels.

The measurements of resistivity, magnetic susceptibility as well as more bulk-sensitive techniques, such as thermal expansion, heat capacity and neutron and x-ray diffraction etc. would allow for an accurate determination of the phase diagrams of the iron-based superconductors. The phase diagrams of three representative iron-based superconductors are shown in Fig. 10. One of the most fascinating phenomena is the apparent coexistence and competition between superconductivity and the SDW phase in the underdoped regime of $Ba(Fe_{1-x}Co_x)_2As_2$. The transition from the SDW phase to superconductivity in $LaFeAs(O_{1-x}F_x)$ appears more abrupt. Such coexistence between superconductivity and magnetism has also been observed in the hole-doped $Ba_{1-x}K_xFe_2As_2$. The exact nature of this phenomenon remains to be established.

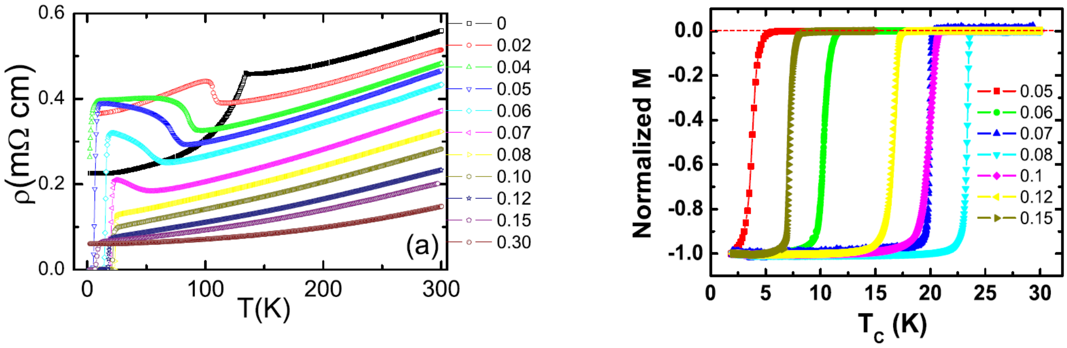

(a) (b)

Fig. 9: *(a) The temperature dependence of (a) the resistivity and (b) the magnetization of the electron-doped Ba(Fe$_{1-x}$Co$_x$)$_2$As$_2$ single crystals [24].*

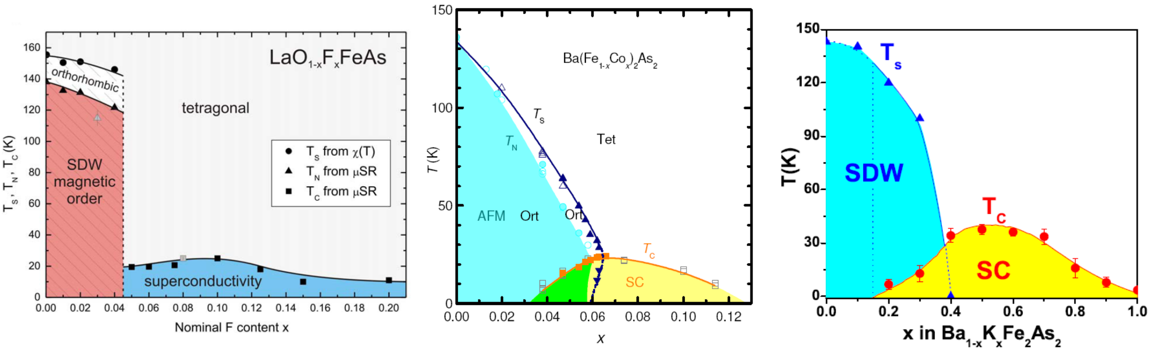

(a) (b) (c)

Fig. 10: *(The phase diagram of: (a) LaFeAs(O$_{1-x}$F$_x$)[23]; (b) Co-doped Ba(Fe$_{1-x}$Co$_x$)$_2$As$_2$ [25]; (c) Ba$_{1-x}$K$_x$Fe$_2$As$_2$. [23]*

4.2 Close proximity to magnetism: magnetic ordering and spin fluctuations

The nature of the magnetic ordering and spin fluctuations in superconductors has had a rich and interesting history, and has been a topic of special interest ever since the parent compounds of the high-T_c cuprates were found to be antiferromagnetic Mott insulators that exhibit huge exchange energies within the Cu-O planes. These strongly correlated spin fluctuations persist into the superconducting regime, often developing a spin resonance mode whose energy scales with T_c and whose intensity exhibits a superconducting order-parameter-like behavior. Recently discovered iron-based superconductors represent another remarkable example in which superconductivity is in close proximity to magnetism. Although neutrons do not couple directly to the superconducting order parameter, they have nevertheless played a decisive role in the understanding of the interplay between superconductivity and magnetism, as demonstrated by the determination of magnetic ordering in the parent compound and the observations of the spin resonant mode in the superconducting counterparts. It has also been established via neutron scattering that magnetic ordering in iron pnictides is strongly coupled to lattice instabilities.

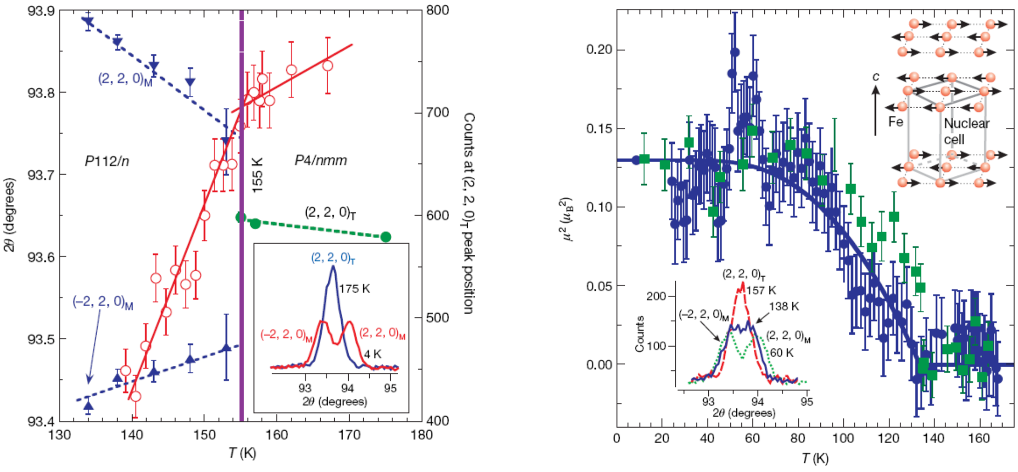

(a) **(b)**

Fig. 11: *Powder neutron diffraction of LaFeAsO [26] : (a) a tetragonal-to-orthorhombic transition occurs at 155 K; (b) an antiferromagnetic ordering due to SDW occurs at 138 K.*

As shown in Fig. 11, the coupling of the antiferromagnetic and structural phase transitions in LaFeAsO has been captured via powder neutron diffraction [26]. This allowed for the determination of long-range collinear antiferromagnetic ordering with a very small saturation moment of 0.4 μB per Fe site.

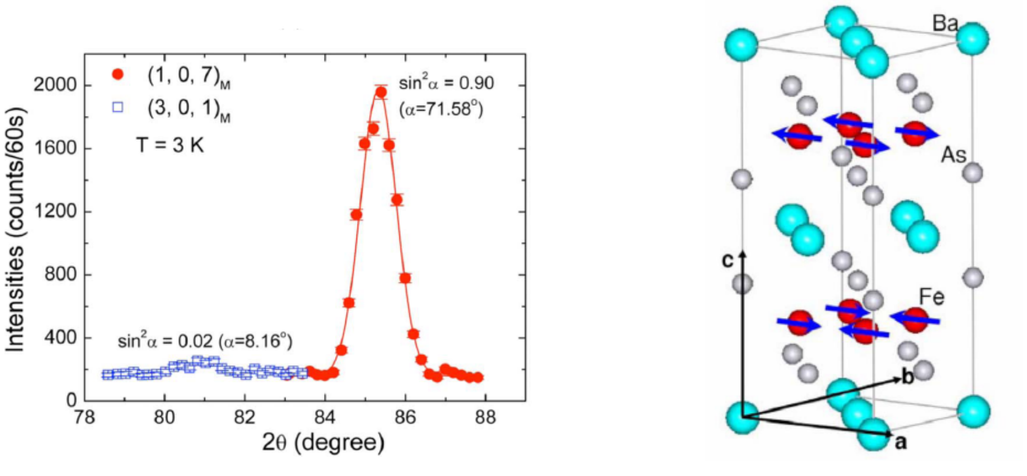

(a) **(b)**

Fig. 12: *Neutron diffraction of single-crystalline $BaFe_2As_2$: (a) the measurement of two magnetic reflections, the clues about the aligning direction of the ordered magnetic moment can be obtained from the drastically different peak intensities; (b) the determined magnetic structure of $BaFe_2As_2$ [27].*

Such a collinear antiferromagnetic ordering was soon after confirmed in single-crystalline $BaFe_2As_2$ [27] and other iron pnictide compounds [23]. As shown in Fig. 12(a), from the measurement of these two magnetic reflections with a modulation wavevector (1, 0, 1), the clues about the aligning direction of the ordered magnetic moment can be obtained from the drastically different peak intensities. The ordered magnetic moment of iron has been determined to be aligned along the longer a-axis of the low temperature orthorhombic phase. The magnetic moments of iron are arranged in such a way that they are anti-parallel to the neighbouring ones along the orthorhombic a- and c-axis, while they are parallel along b-axis (in Fig. 12(b)). Except the case in the parent compound of iron chalcogenides family, the saturation moments of Fe in all other iron pnictide parent compounds have been found to be in the range of 0.3-1.0 μB.

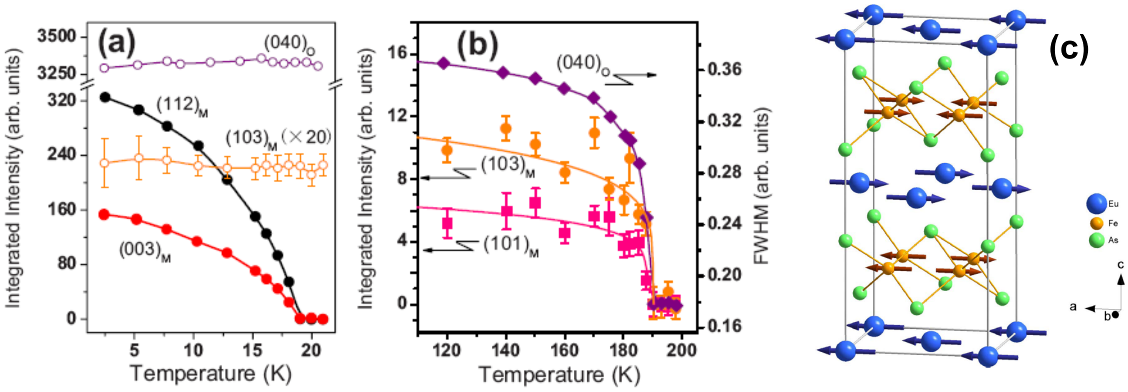

Fig. 13: *The magnetic structure of* $EuFe_2As_2$*: (a)-(b) the temperature dependence of the* Eu^{2+} *antiferromagnetic reflections* $(112)_M$ *and* $(003)_M$ *and the Fe-SDW reflections* $(101)_M$ *and* $(103)_M$*; (c) the refined magnetic structure [28].*

However, the determination of magnetic structures in some magnetic rare-earth containing iron pnictide compounds is not trivial due to the presence of two magnetic sublattices as well as the possible interplay between the localized rare-earth magnetism and itinerant Fe-SDW, such as in $EuFe_2As_2$ [28] and SmFeAsO [29] etc. Via complementary single-crystal neutron and magnetic x-ray scattering, the magnetic structure of $EuFe_2As_2$ has been thoroughly determined [28](see Fig. 13). The Fe-SDW retains the same magnetic ordering as in other parent iron pnictides, the the Eu^{2+} moment is aligned along the orthorhombic **a**-axis. The propagation wavevector of the Eu^{2+} antiferromagnetic ordering is $\mathbf{Q}_{Eu}$ = (0, 0, 1) with T_N = 19 K, while the Fe-SDW orders at $\mathbf{Q}_{SDW}$ = (1, 0, 1) with T_{SDW} = 190 K. The temperature dependence of the corresponding magnetic reflections indicates a rather weak coupling between these magnetic sublattices. The situation appears quite differently in SmFeAsO, in which a strong coupling between Sm and Fe magnetism has been experimentally demonstrated [29].

While the static magnetic ordering in various iron pnictides compounds has been well established, the nature of magnetism is being hotly debated. Two approaches have been used so far, one based on the localized Heisenberg J_1-J_2 exchange interactions, the other based on the itinerant picture where magnetism is governed by the Fermi surface (FS) nesting wavevector between the hole pockets at the Γ-point and the electron pockets at the M-point (as schematically shown in Fig. 14). A recent inelastic neutron scattering investigation on the spin-wave excitations of $CaFe_2As_2$ [30] indicated that the spin waves in the entire Brillouin zone can be described by an effective three-dimensional local-moment Heisenberg Hamiltonian, but the large in-plane anisotropy cannot. Therefore, magnetism in the parent compounds of iron arsenide superconductors was suggested to be neither purely local nor purely itinerant, rather it is a complicated mixture of the two.

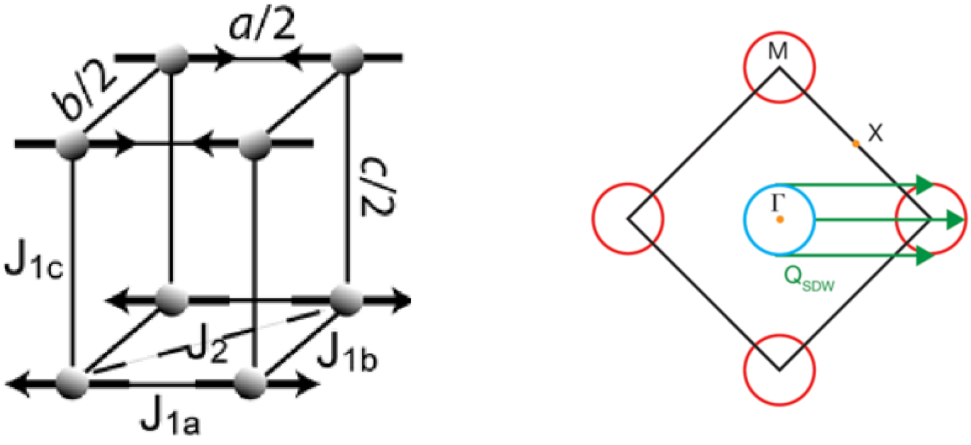

(a) **(b)**

Fig. 14: *The nature of magnetism in iron-based superconductors: (a) Heisenberg J_1-J_2 exchange interactions based on the well localized spins; (b) Interband particle-hole excitation due to the Fermi surface nesting.*

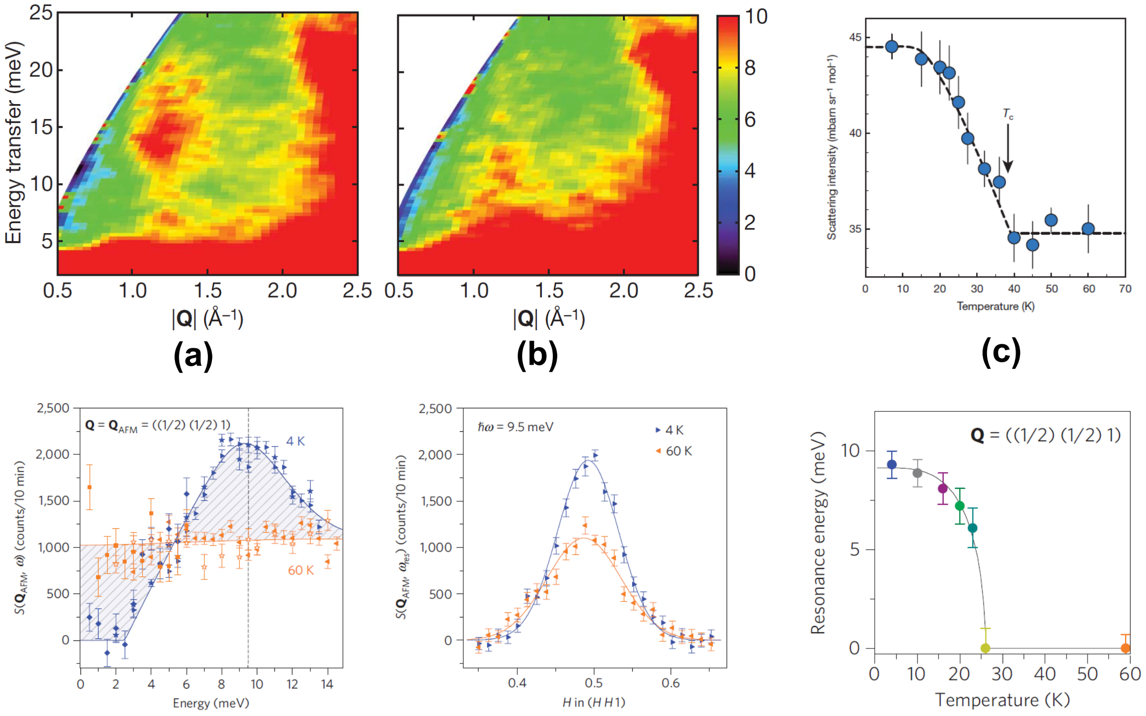

(a) **(b)** **(c)**

(d) **(e)** **(f)**

Fig. 15: *The spin resonance mode observed via inelastic neutron scattering techniques: (a-c) in $Ba_{1-x}K_xFe_2As_2$ via time-of-flight spectroscopy [31]; (d-f) in $Ba(Fe_{1-x}Co_x)_2As_2$ via triple-axis spectroscopy [32].*

Measurements of the spin dynamics within the spin density wave phase of the parent compounds has shown evidence of strongly dispersive spin waves with exchange interactions consistent with the observed magnetic order and a large anisotropy gap. Again, in a way very similar to the cuprates, these antiferromagnetic spin fluctuations persist in the normal state of the superconducting compounds, but they become more diffuse. Below T_c, there exists evidence in several "122" compounds that these spin fluctuations condense into a resonant spin excitation at the in-plane antiferromagnetic wavevector with an energy that scales with T_c (see Fig. 15) [31, 32, 23] . Such resonances have been also observed in the high-T_c cuprates and a number of heavy fermion superconductors, where they are considered to be the evidence of d-wave symmetry. Since it has been indicated from ARPES and other measurements that the superconducting gap in iron-based superconductors is likely isotropic, the observation of the spin resonance mode in neutron scattering has thus been seen as strong evidence of unconventional superconductivity due to sign-reversal $s_{\pm}$-wave symmetry.

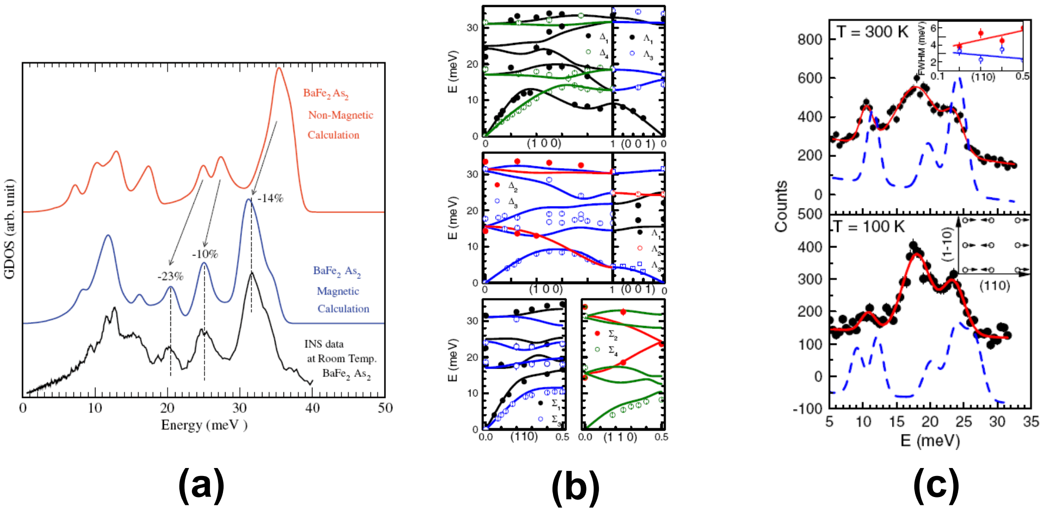

Fig. 16: *(a) Generalized phonon-DOS measured by inelastic neutron scattering at room temperature for BaFe$_2$As$_2$ (bottom black curve) and the calculated GDOS with (middle blue) and without (top red) Fe-magnetism [33]; (b) comparison of experimentally determined phonon frequencies (solid circles) in the (100), (001) and (110) directions of CaFe$_2$As$_2$ at T = 300 K with the results of density functional theory (solid lines)[34]; (c) anomalous phonons in CaFe$_2$As$_2$ measured at Q = (2.5, 1.5, 0) at room temperature and at a temperature far below the structural phase transition. The calculated phonon structure factors for nonmagnetic and spin-polarized are shown in the upper and lower panel (dashed lines), respectively [34].*

4.3 Roles of electron-phonon coupling

It has been widely accepted that electron-phonon coupling alone can not account for the occurrence of high temperature superconductivity in iron-based superconductors [35]. However, the importance of electron-phonon coupling have been implied from a number of experiments. As shown in Fig. 16(a), the generalized phonon density-of-state (DOS) measured by inelastic neutron scattering at room temperature for BaFe$_2$As$_2$ is much closer to the calculated magnetic phonon-DOS rather than non-magnetic one [33]. This clearly demonstrates that the Fe-magnetism is intimately coupled to the phonons in iron pnictides. One way to verify possible roles of electron-phonon coupling is to measure phonon dispersions as a function of temperature in details on single-crystal sample via inelastic neutron scattering. A fairly complete picture of phonon dispersions in the main symmetry directions of $CaFe_2As_2$ has been established from such an approach [34], as shown in Fig. 16(b). Strong temperature dependence of some phonons near the structural phase transition near 172 K was observed (see Fig. 16(c)). The calculated phonon spectra for non-magnetic/spin-polarized structures are shown as dashed lines in Fig. 16(c). The agreement between the experimental results and the calculation is poor. It has been suggested that the interplay between magnetism and the lattice is in some way responsible for the anomalous phonons in $CaFe_2As_2$. That is to say, the coupling of the vibrational and the electronic degrees of freedom is stronger than calculated by density functional theory, and hence phonon might play an important role in superconductivity in the doped compounds.

4.4 Superconducting gap symmetry and structure

Understanding the nature of the superconducting gap (Δ) in a superconductor is essential to establish the microscopic origin of superconductivity, since the magnitude, symmetry and structure of a superconducting gap are directly associated with the pairing strength and the pairing interactions. For instance, the wider the gap, the harder it is to break apart the Cooper pairs and destroy the superconducting state. In conventional superconductors (e.g. Nb, Pb and Al etc.), the superconducting gap function, that can be nicely predicetd by the BCS theory, has *s*-wave symmetry and it is thus isotropic along the Fermi sea (as schematically shown in Fig. 17(a)). This reflects the pairing interaction being attractive, its origin is the electron-electron interaction mediated by phonons. *p*-wave pairing symmetry has been suggested for superfluid ^{3}He and possibly in ruthenates superconductors. The pairing symmetry for the high-TC cuprates has been identified to be *d*-wave. The gap nodes, where the superconducting gap can be closed, exist for both *p*-wave and *d*-wave (see Fig. 17(b)-(c)).

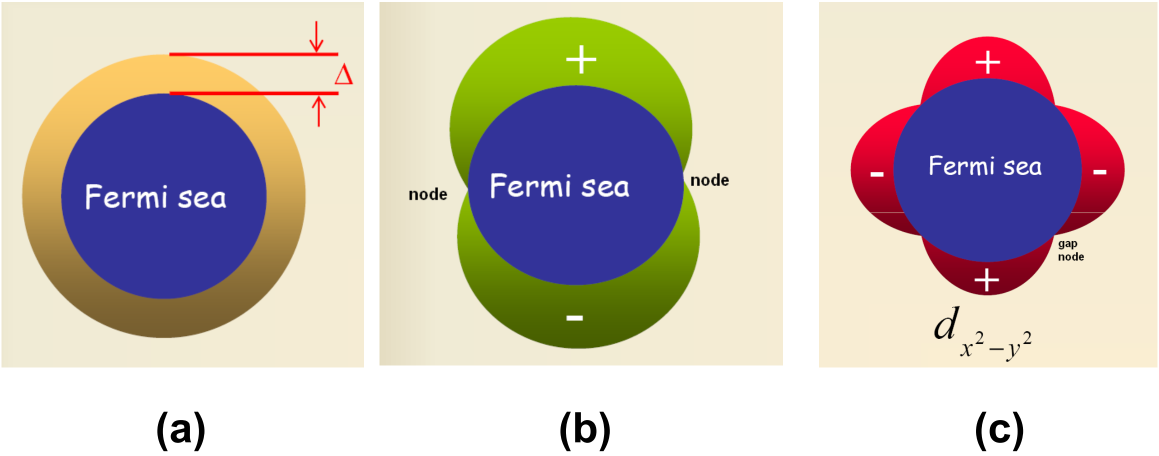

Fig. 17: *The schematic drawing of the superconducting gap functions: (a)* s*-wave, nodeless isotropic gap; (b)* p*-wave, with nodes; (c)* d*-wave, with nodes.*

One of the key challenges for iron-based superconductors is to identify the superconducting gap symmetry and structure. While the leading candidate for the pairing symmetry in iron-based superconductors is a sign-reversal $s_{\pm}$-wave as first proposed by Mazin[36], unlike the case in cuprates, an unambiguous picture has not been established [23]. It has been found that the superconducting gap seemingly shows strong material dependence. As an example shown in Fig. 18, two isotropic gaps can be identified in hole-doped $Ba_{0.6}K_{0.4}Fe_2As_2$ via ARPES [37].

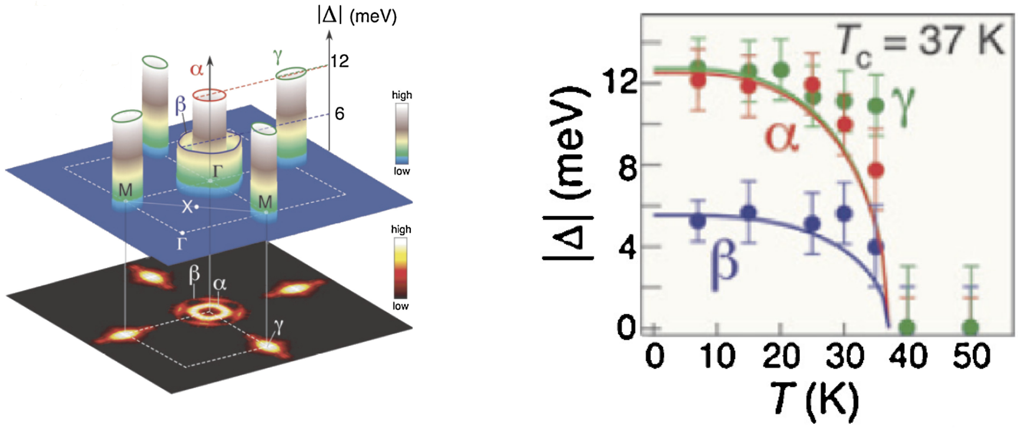

(a) **(b)**

Fig. 18: *Fermi-surface-dependent nodeless superconducting gaps in* $Ba_{0.6}K_{0.4}Fe_2As_2$*: (a) three-dimensional plot of the superconducting gap amplitude (*Δ*) measured at 15 K on the three observed Fermi surface sheets (shown at the bottom as an intensity plot); (b) their temperature evolutions [37] .*

5 Special topics

5.1 Superconducting vortex lattices

For type-II superconductors with $\lambda \geqslant 1/\sqrt{2}\,\xi$, the magnetic flux can penetrate the superconductor and form the vortices. The superconducting order parameter will be suppressed over the core region of the length scan ξ and the supercurrent surrounding the vortex core will extend over the length scale λ. To minimize the total free energy of the system, these vortices will arrange themselves in a periodic array, which is called Abrikosov flux line lattice (FLL). Many important information concerning the superconducting state, such as penetration depth and coherence length can be obtained by investigating the flux line lattice [38].

Among many experimental techniques, Small Angle Neutron Scattering (SANS) is considered as one of the most suitable probe for flux line lattice because neutrons can be scattered via the interaction of their intrinsic moments with the modulation of magnetic field originated from the flux line lattice. The diffraction pattern from SANS provides not only the information about the structure of flux line lattice and its correlation with the crystal lattice, but also the information on the gap structure and the value of characteristic length scales [39].

In Fig. 19, series of SANS diffraction patterns from the flux line lattice of $YBa_2Cu_3O_{7-\delta}$ cuprate superconductor are presented [40]. these patterns are collected at 2 K and various magnetic field along the crystallographic c axis. It can be seen that hexagonal FLL structure is formed at 1.5

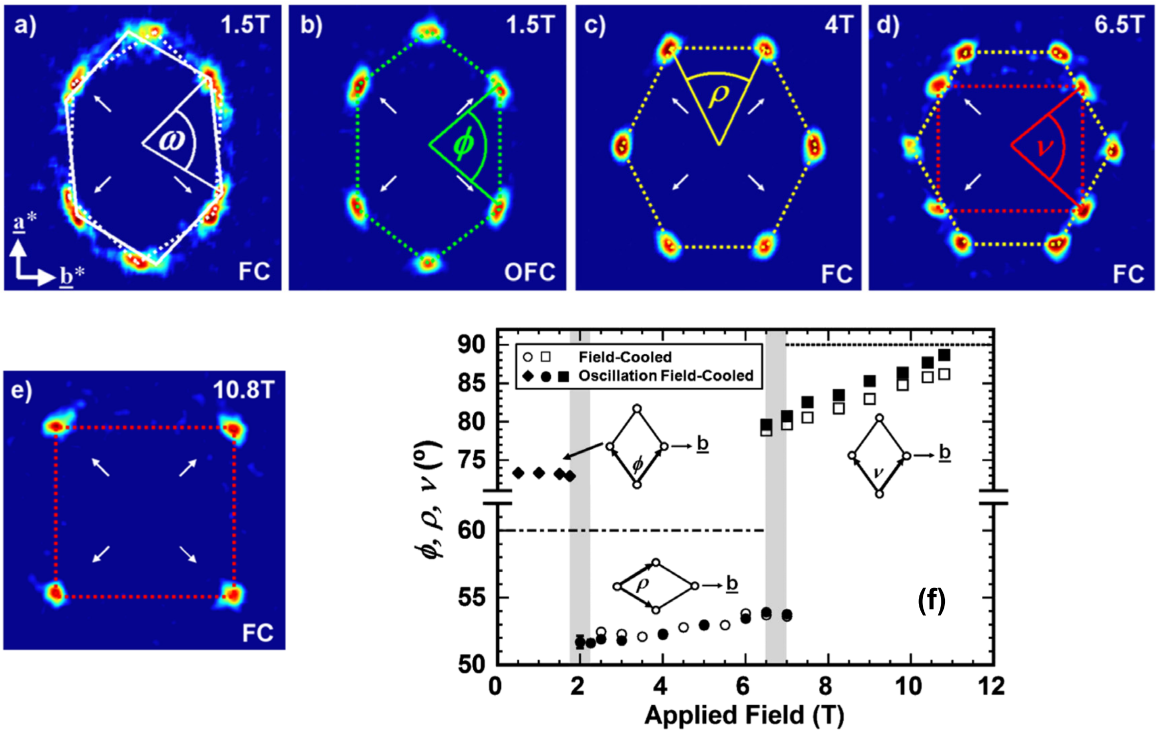

Fig. 19: *(a) to (e) Flux line lattice diffraction patterns of* $YBa_2Cu_3O_{7-\delta}$ *cuprate superconductor taken at 2 K in different magnetic fields. FC and OFC indicate field cooling and oscillation field cooling procedures, respectively. (f) Magnetic field dependence of the flux line lattice apex angle for different structure type [40].*

T [Fig. 19(a) and (b)]. When 4 T field is applied, a single distorted hexagonal FLL is observed. The transition between these two hexagonal FLL is likely to be first order as indicated by sudden change of FLL symmetry angle [see Fig. 19(f)]. Another first order FLL structure transition is observed with further increase of field. As shown in Fig. 19(d), the rhombic FLL structure emerges and coexists with the distorted hexagonal structure at 6.5 T. Once field reached above 7 T, the pure rhombic structure is established for the FLL.

In the simplest approximation, hexagonal flux line lattice is the most stable state due to the close packed structure. However, repulsive interaction between the flux line, property of the Fermi surface, as well as the anisotropic superconducting order parameter can result in the transition from hexagonal to other symmetry. As described above, two field driven first order flux line lattice structure transitions was observed in $YBa_2Cu_3O_{7-\delta}$. It is suggested that the low field transition is probably driven by Fermi surface effects, while the high field transition from hexagonal to square structure is due to the dominant role of anisotropic superconducting order parameter.

5.2 Crystal field excitation in superconductors

For the rare earth ions, both electric field and magnetic field can lift, at least partially lift the $2J$+1 fold degenerate ground state. Considering a three dimentional crystal structure, the electric field might be generated by the ion surrounding the rare earth ion in lattice. Following some definitions and transformations, crystal electric field (CEF) Hamiltonian can be expressed as this famous notation, $\mathcal{H}_{CEF} = \sum_{l,m} B_l^m O_l^m$, where B_l^m is the crystal field parameters and O_l^m is the Stevens equivalent operators. It is obvious that the crystal field Hamiltonian will give rise to discrete energy levels. Neutron scattering is the method of choice to determine crystal field level schemes by measuring the excitation between these levels. The magnetic scattering of the CEF transition can be expressed in terms of differential neutron cross section. Because CEF of rare earth is largely related to the surrounding environment, to study the CEF of rare earth in rare earth based superconductor can provide detailed information on the local charge distribution and the formation of energy gap.

Inelastic neutron scattering has been long time used to investigate the relaxation behavior of the ground state crystal field excitation associated with the rare earth ion in high T_c cuprate superconductor. Since the crystal field levels are subject to an interaction with charge carriers, neutron scattering measurements of the relaxation rate of crystal field excitations can provide the direct evidence on the opening of energy gap and reflect the variation of density of state at the Fermi energy. For example, the pseudogap opening temperature in Ho-based cuprate can be clearly observed by following the emperature dependence of the intrinsic linewidth corresponding to the lowest ground state crystal field excitation [41].

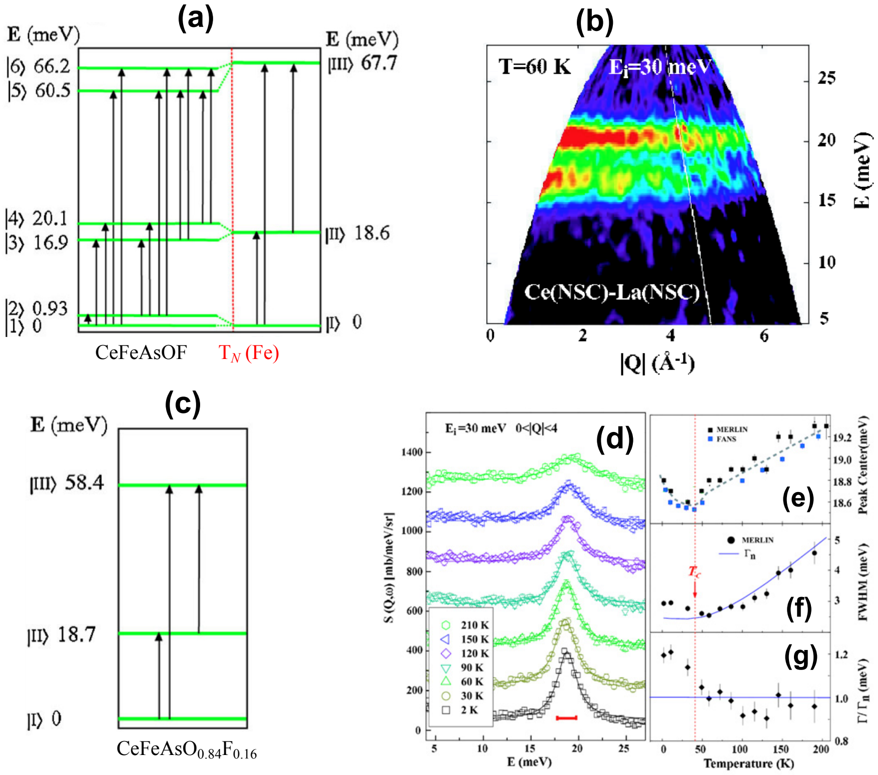

Fig. 20: *(a) Energy level scheme of* Ce^{3+} *ion in CeFeAsO as determined by inelastic neutron scattering. (b)Energy spectra of neutron scattered from CeFeAsO at* $T = 60$ *K. Noted that the phonons contribution collected using isostructural LaFeAsO compound was substracted. (c) Energy level scheme of* Ce^{3+} *ion in* $CeFeAsO_{0.84}F_{0.16}$ *as determined by inelastic neutron scattering. (d) Temperature dependence of excitation between ground state and the first excited state in* $CeFeAsO_{0.84}F_{0.16}$. *(e) Temperature dependence of the peak position (e), intrinsic line width (f), line width ratio (g) for the excitation peak in (d) [42].*

Regarding to the recently discovered Fe-pnictide superconductor, there also exist a large number of compounds that content rare earth elements, such as RFeAs($\mathrm{O}_{1-x}\mathrm{F}_x$) compounds with R = Ce, Nd, Sm, or Pr etc. As we will show in the following example, the crystal electric field can be used as a probe for long range antiferromagnetic order and superconducting state in $\mathrm{CeFeAsO}_{1-x}\mathrm{F}_x$ superconductors [42].

Similar to other parent compounds of Fe-pnictides, CeFeAsO exhibits a phase transition from tetragonal to orthorhombic structure and then orders antiferromagneticly with decreasing temperature. The crystal field Hamiltonian for two different structures can be written as $\mathcal{H}_{(T)} = B_2^0 O_2^0 + B_4^0 O_4^0 + B_4^4 O_4^4$ and , $\mathcal{H}_{(O)} = B_2^0 O_2^0 + B_2^2 B_2^2 + B_4^0 O_4^0 + B_4^2 O_4^2 + B_4^4 O_4^4$, respectively. The crystal field parameters B_l^m can be deduced by modeling the inelastic neutron scattering data. It was found that three doublets are shown in paramagnetic phase of CeFeAsF, and these three doublets split into six singlet when the Fe ions order antiferromagneticlly. The splitting scheme of crystal electric field is shown in Fig. 20(a). A typical inelastic neutron spectra of CeFeAsF collected at 60 K is presented in Fig. 20(b), in which two clear bands of CEF excitations at 16.9 and 20.1 meV are clearly observed.

For F-doped $\mathrm{CeFeAsO}_{0.84}\mathrm{F}_{0.16}$ superconductor, the tetragonal structure maintains in wide temperature range from 4 K to room temperature. Three doublets are detected [Fig. 20(c)]. In Fig. 20(d), the excitation between the ground state and the first excited state is plot as a function of temperature. The temperature dependence of peak position, intrinsic line width are obtained by fitting the excitation peaks [Fig. 20(e),(f) and (g)]. Both peak position and line width exhibit anomalies at critical temperature T_c at around 40 K, which suggested that CEF can be used as a probe for the superconducting state in Fe-pnictide superconductors.

6 Summary

While high temperature superconductivity remains one of the biggest challenges in condensed matter physics, the understanding of its mechanism has advanced tremendously over the past 26 years or so. A common feature among cuprates, iron-based superconductos and heavy-fermion superconductors is that superconductivity is in close proximity to magnetism. This has thus provided neutron scattering with an important playground due to its unique sensitivity to magnetic correlations in a wide dynamic range as demonstrated in previous sections. It can be expected that the advanced scattering methods in particular neutron scattering will continue to play a major role in the studies of superconductivity.

References

[1] H. K. Onnes, Leiden Commun. **120b, 122b, 124c** (1911).

[2] J. G. Bednorz and K. A. Müller, Zeitschrift für Physik B Condensed Matter **64**, 189 (1986).

[3] Y. Kamihara *et al.*, J. Am. Chem. Soc. **130**, 3296 (2008).

[4] C. Kittel, *Introduction to Solid State Physics* (John Wiley & Sons, Inc. New York, 2004).

[5] P. Hofmann, *Solid State Physics* (Wiley-VCH, Berlin, 2008).

[6] W. Meissner and R. Ochsenfeld, Naturwissenschaften **21**, 787 (1933).

[7] F. London and H. London, Proceedings of the Royal Society of London. Series A - Mathematical and Physical Sciences **149**, 71 (1935).

[8] V. L. Ginzburg and L. D. Landau, Zh. Eksp. Teor. Fiz. **20**, 1064 (1950).

[9] A. A. Abrikosov, Sov. Phys. JETP **5**, 1174 (1957).

[10] J. Bardeen, L. N. Cooper, and J. R. Schrieffer, Phys. Rev. **108**, 1175 (1957).

[11] F. J. Owens and J. Charles P. Poole, *The new superconductors* (Plenum Press, 1996).

[12] J. Nagamatsu *et al.*, Nature **410**, 63 (2001).

[13] T. Ishiguro, K. Yamaji, and G. Saito, *Organic Superconductors* (Springer, 1998).

[14] C. Pfleiderer, Rev. Mod. Phys. **81**, 1551 (2009).

[15] A. Hebard, Nature **350**, 600 (1991).

[16] A. Y. Ganin, Nature Materials **7**, 367 (2008).

[17] http://en.wikipedia.org/wiki/Superconductivity .

[18] M. K. Wu *et al.*, Phys. Rev. Lett. **58**, 908 (1987).

[19] A. Schilling, M. Cantoni, J. D. Guo, and H. R. Ott, Nature **363**, 56 (1993).

[20] P. C. Canfield, Nature Materials **10**, 259 (2011).

[21] K. A. Moler, Nature **468**, 643 (2010).

[22] V. J. Emery, S. A. Kivelson, and J. M. Tranquada, Proc. Natl. Acad. Sci. USA **96**, 8814 (1999).

[23] D. C. Johnston, Advances in Physics **59**, 803 (2010).

[24] L. Fang *et al.*, Phys. Rev. B **80**, 140508(R) (2009).

[25] S. Nandi *et al.*, Phys. Rev. Lett. **104**, 057006 (2010).

[26] C. de la Cruz *et al.*, Nature **453**, 899 (2008).

[27] Y. Su *et al.*, Phys. Rev. B **79**, 064504 (2009).

[28] Y. Xiao *et al.*, Phys. Rev. B **80**, 174424 (2009).

[29] S. Nandi *et al.*, Phys. Rev. B **84**, 054419 (2011).

[30] J. Zhao *et al.*, Nature Physics **5**, 555 (2009).

[31] A. D. Christianson *et al.*, Nature **456**, 930 (2008).

[32] D. S. Inosov *et al.*, Nature Physics **6**, 178 (2010).

[33] M. Zbiri *et al.*, Phys. Rev. B **79**, 064511 (2009).

[34] R. Mittal *et al.*, Phys. Rev. Lett. **102**, 217001 (2009).

[35] L. Boeri *et al.*, Phys. Rev. Lett. **101**, 4 (2008).

[36] I. I. Mazin *et al.*, Phys. Rev. Lett. **101**, 057003 (2008).

[37] H. Ding *et al.*, Europhys. Lett. **83**, 47001 (2008).

[38] R. P. Huebener, N. Schopohl, and G. E. Volovik, *Vortices in unconventional superconductors and superfluids* (Springer, 2002).

[39] M. R. Eskildsen, Front. Phys. **6**, 398 (2011).

[40] J. S. White *et al.*, Phys. Rev. Lett. **102**, 097001 (2009).

[41] A. Furrer, *Neutron Scattering Investigations of Charge Inhomogeneities and the Pseudogap State in High-Temperature Superconductors* (Springer, 2005).

[42] S. Chi *et al.*, Phys. Rev. Lett. **101**, 217002 (2008).